http://doi.org/10.1016/j.jfoodeng.2014.06.016

Numerical study on spout elevation of a gas-particle spout fluidized bed in microwave-vacuum dryer

Guangyuan Jin [a,b], Min Zhang [a,b]*, Zhongxiang Fang[c*], Zhengwei Cui[b], Chunfang Song[b]

[a] *State Key Laboratory of Food Science and Technology, Jiangnan University, Wuxi, Jiangsu, China*

[b] *Jiangsu Province Key Laboratory of Advanced Food Manufacturing Equipment and Technology, Jiangnan University, China*

[c] *School of Public Health, Curtin Health Innovation Research Institute, International Institute of Agri-Food Security, Curtin University, Bentley, Western Australia, WA 6102, Australia*

*Corresponding authors: Tel.: +86-510-85877225; Fax: +86-510-85877225;

E-mail: min@jiangnan.edu.cn(M. Zhang). Tel.: +61 8 9266 2470; Fax: +61 8 9266 2958, zhongxiang.fang@curtin.edu.au(Z. X. Fang)

Abstract:

The dynamic characteristics of gas-particle spout fluidized bed in a pulsed spouted microwave-vacuum drying system (PSMVD) were investigated. The spout fluidization process in a pseudo-2-D spout fluidized bed was simulated by computational fluid dynamics (CFD) using the inviscid two-fluid theory method (TFM) based on the kinetic theory of granular flow. The dynamic characteristics of the spout fluidized bed and the effect of spout elevation on the particle movement were revealed, which could be used to improve the uniformity of particle mixing and microwave heating. The mathematical model demonstrated that the spout fluidization process includes isolated, merged and transitional jets and the fluidization at a specific spout gas velocity has a start-up stage and a quasi-steady fluidization stage. The spout velocity was an important factor controlling particle status in the spout fluidized bed and a critical velocity was identified for effect transition of the flow pattern. There was an approximately linear correlation between the jet penetration depth and the spout velocity. When the spout gas velocity increased up to the critical velocity region, the pressure drop tended to convert from negative pressure to positive pressure.

Keywords: Microwave-vacuum dryer; Spout fluidized bed; Fluid dynamics; CFD model

Nomenclature		Δt	time step (s)
C_D	drag force coefficient	$\vec{u}$	velocity vector (m/s)
d_p	particle diameter (m)	u_{spout}	spout velocity (m/s)
$\vec{F}$	net force (N/m^3)	Greek symbols	
		ε	volume fraction
g	acceleration due to gravity (m/s^2)	ρ	density (kg/m^3)
H	bed height (m)	μ	viscosity (Ns/m^2)
L	nozzle width (m)	Subscripts	
P	pressure (N/m^2)	g	gas
ΔP	bed pressure drop (N/m^2)	p	particle
Re	Reynolds number		
t	time (s)		

1. Introduction

In recent years, microwave-vacuum drying (MVD) has been tentatively applied in food industry as a potential drying method for obtaining high quality food products, including dried fruits, vegetables and grains (Zhang et al. 2010, Li et al. 2011). MVD possesses the advantages of both microwave heating and vacuum drying. The combination of low temperature and fast mass transfer conferred by vacuum drying and rapid energy transfer by microwave heating generates a very rapid, low temperature drying process and has the potential to improve energy efficiency and product quality. Although MVD can offer unique advantages, the inherent problem preventing its widespread application is the nonuniform temperature distribution caused by uneven spatial distribution of the electromagnetic field inside the drying cavity, which results in hot and cold spots in the dried product (Li et al, 2011). The nonuniform temperature distribution in microwave drying also causes an issue of microbial safety in food products (Vadivambal et al. 2010, Jangam et al. 2011).

The heating uniformity of MVD is influenced by many factors, such as vacuum cavity effects, product physical attributes and geometry, spatial location, and spatial electromagnetic field intensity in the microwave cavity (Zhang et al. 2006, 2010). Many researchers have studied the MVD characteristics of food materials, both experimentally (Hu et al. 2006, Huang et al. 2011, Nahimana et al. 2011) and theoretically using analytical and mathematical methods (Giri et al. 2007, Han et al. 2010, de Jesus et al. 2011). Various field-averaging methods have been developed to achieve the heating uniformity. The MW energy averaging can be accomplished by either mechanical means (Torringa et al. 1996) or through pneumatic agitation (Feng et al. 1998; Balakrishnan et al. 2011).

Fluidization provides a pneumatic agitation for particles in the drying bed. It also facilitates heat and mass transfers due to a constantly renewed boundary layer on the particle surface (Feng et al. 2001, Jambhale et al. 2008). Therefore, combination of fluidized or spouted bed drying with MVD is considered as an effective means of solving the uneven heating problem. It is well known that coarse food particles such as diced or sliced materials are difficult to be fluidized by a conventional fluid bed, especially when their moisture content is relatively high and surface is sticky. However, pulsed spouted bed can be used for fluidizing the coarse particles. Although a few researchers have performed some experimental investigations on the drying characteristics of food materials by this new technique (Wang et al. 2012, 2013), more work about fluidization need to conducted to understand the drying mechanism in pulsed spouted microwave-vacuum drying (PSMVD).

Computational fluid dynamic (CFD) approach has been recognized as a useful tool to obtain detailed hydrodynamics of a complex gas-solid flow (Rahimi et al. 2013). Two different methods are generally used for modeling dispersed phase flows in fluidized and spouted bed, namely, Eulerian-Eulerian (EE) and Eulerian-Lagrangian (EL) methods (Pai and Subramaniam 2009). In EL or discrete element method (DEM), the continuous phase flow is evaluated by Eulerian approach, while the individual particle trajectories are evaluated by Lagrangian approach. Although the EL approach requires less modeling assumption for the particulate phase, it requires highly efficient computation to analyze dense gas-solid fluidized beds (Pritchett et al. 1978, Bouillard et al. 1989). Two-fluid model (TFM) based on the EE method is a popular approach requiring smaller CPU and memory resources, and has been used in a large number of studies (Gidaspow et al. 1994, 2004). In the TFM model, the two phases are treated as interpenetrating continua. This approach has been successfully utilized for predicting and validating hydrodynamics of the gas-solid systems. For example, Passalacqua and Marmo (2009) used the TFM to predict bubble diameter in a bubbling fluid bed with a central jet and the bubble diameter distribution in a uniformly fed bubbling fluidized bed. Zhong et al. (2010), Wang et al. (2007) and Pei et al. (2009) have also applied the TFM in studying hydrodynamics of spout-fluid bed, fluidized bed coal gasification, circulating fluidized beds and jet fluidized beds, respectively. The success of a TFM depends on the proper description of the interfacial forces and the constitutive models for solid and fluid stresses. The interfacial forces are used to describe the momentum transfer between the phases, which significantly affects the hydrodynamic behavior of the two-phase flows.

In the present study, the effect of combining a pseudo two-dimensional spout fluidized bed in a pulsed spouted microwave-vacuum drying system (PSMVD) was investigated using the TFM method. The dynamic characteristics of the gas-particle spout fluidized bed and the effect of spout elevation on particle movement at different spout gas velocity conditions were revealed, which could be used to improve the uniformity of particle mixing and heating in a PSMVD system.

2. PSMVD equipment and materials

2.1. PSMVD equipment

An experimental equipment was designed in our laboratory for the PSMVD study, which consisted of the following seven basic components. The schematic diagram of the PSMVD system was shown in Figure 1.

(1) a cylindrical multimode microwave cavity (Figure.1-3), equipped with four microwave generators (at 2,450 MHz);

(2) a circular duct vacuum drying chamber (Figure.1-6);

(3) a pulse-spouted system (Figure.1-11,12,13,14), equipped with a set of adjustable gas flow and distributive unit as well as a set of air handing units of 1m3/min capacity;

(4) a heat supply system (Figure.1-4). Each magnetron's power output was in the range of 0.1 to 1.0kW by a GPA-1800W microwave power controller;

(5) a water load system (Figure.1-5), which was added to prevent the magnetron from overheating;

(6) a vacuum system (Figure.1-7,8,9,10) equipped with a cooler and a water-ring vacuum pump with a pumping rate of 1m3/min.

The pressure inside the drying chamber could be regulated in the range of 3.5 to 100 kPa.

<Figure 1>

2.2. Materials

Fresh stem lettuce (*Lactuca sativa*) obtained from Haitong Food Group farm in Ningbo city, China, was used as a model drying material. In this study, the lettuce particle is simplified as spherical particle with a diameter of 5 mm. The physical properties of lettuce dices were measured and the details were shown in Table 1, which represented a typical food particle for drying (Wang et al. 2012).

3. Computational models and method

3.1. The hydrodynamic model

In the present study, the inviscid two-fluid theory (Gidaspow 1994; 2004) was used to investigate both the fluid and particle movements in a gas-solid spout fluidized bed under vacuum pressure conditions. The continuity and momentum equations of describing gas and particle flows are given below:

Continuity equations:

Particle phase
$$\frac{\partial \varepsilon_p}{\partial t} + \nabla \cdot \left(\varepsilon_p \vec{u}_p \right) = 0 \quad (1)$$

Gas phase
$$\frac{\partial \varepsilon_g}{\partial t} + \nabla \cdot \left(\varepsilon_g \vec{u}_g \right) = 0 \quad (2)$$

Momentum equations:

Particle phase
$$\frac{\partial \left(\varepsilon_p \rho_p \vec{u}_p \right)}{\partial t} + \nabla \cdot \left(\varepsilon_p \rho_p \vec{u}_p \vec{u}_p \right) = \vec{F}_{p,net} \quad (3)$$

Gas phase
$$\frac{\partial \left(\varepsilon_g \rho_g \vec{u}_g \right)}{\partial t} + \nabla \cdot \left(\varepsilon_g \rho_g \vec{u}_g \vec{u}_g \right) = \vec{F}_{g,net} \quad (4)$$

Where ε represents the volume fraction ($\varepsilon_p + \varepsilon_g = 1$), *u* is the flow velocity, and $\vec{F}$ is the net force. The subscripts *g* and *p* indicate gas and particle phase, respectively.

Particle-phase force component:

$$\vec{F}_{p,net} = -\varepsilon_p \nabla p + \nabla \cdot \overline{\overline{\tau}}_p + \varepsilon_p \rho_p \vec{g} + \sum_{p=1}^{n} K_{pg} (\vec{u}_p - \vec{u}_g) + \vec{F}_p \quad (5)$$

Gas-phase force component:

$$\vec{F}_{g,net} = -\varepsilon_g \nabla p + \nabla \cdot \overline{\overline{\tau}}_g + \varepsilon_g \rho_g \vec{g} + \sum_{g=1}^{n} K_{gp} (\vec{u}_g - \vec{u}_p) + \vec{F}_g \quad (6)$$

Where *p* is the pressure shared by all phases, $\overline{\overline{\tau}}$ is the phase stress-strain tensor, and K is the momentum exchange coefficient.

Gas-particle momentum exchange is calculated based on the Syamlal-O'Brien model

(Syamlal and O'Brien, 1989):

$$K_{pg} = K_{gp} = \frac{\varepsilon_p \rho_p f}{\tau_p}, \; f = \frac{C_D \mathrm{Re}_p \, \varepsilon_g}{24 u_{r,p}^2} \tag{7}$$

Where $u_{r,p}$ is the terminal velocity correlation for the solid phase (Garside and Al-Dibouni, 1977):

$$u_{r,p} = 0.5(A - 0.06\mathrm{Re}_p + \sqrt{(0.06\mathrm{Re}_p)^2 + 0.12\mathrm{Re}_p(2B - A) + A^2}),$$

$$A = \varepsilon_g^{4.14}, B = \varepsilon_g^{2.65} \quad (\varepsilon_g \geq 0.85) \tag{8}$$

The empirical Dallavalle relation is used to express drag coefficient C_D:

$$C_D = \left(0.63 + \frac{4.8}{\sqrt{\mathrm{Re}_p \, u_{r,p}}}\right)^2, \tag{9}$$

Where Re_p is particle Reynolds number, defined as

$$\mathrm{Re}_p = \frac{\rho_g \left|\vec{u}_p - \vec{u}_g\right| d_p}{\mu_g} \tag{10}$$

Where d_p is particle diameter, and μ_g is gas viscosity.

3.2. Numerical method

Knudsen is a dimensionless parameter of rarefied gas. Because the Knudsen of the vacuum flow (absolute pressure, 7000Pa) in the present PSMVD equipment was far lower than 1, the flow was consistent with fluid continuum hypothesis and solved by the Navier-Stokes equation (Shen, 2005). Simulations of a gas-solid flow in PSMVD equipment were carried out on a CFD package (ANSYS FLUENT, USA). Two-fluid model of Eulerian-Eulerian was used to capture gas-solid flow hydrodynamic.

In the present pseudo two-dimensional spout fluidized bed (pseudo-2D spout fluidized bed), the spouted flow was simplified to a two dimensional flow as shown in Figure 2. The width of the drying chamber was 40 mm and cavity height H 516 mm; the width of air distribution nozzle L was 8 mm and air distributor angle was 45 °. Air and lettuce particle were used as gas and particle phase, respectively (Table 1).

The two dimension flow field was computed with the software of ANSYS FLUENT by solving the Reynolds-Averaged Navier-Stokes equations. An implicit scheme of volume fraction, a laminar viscous model, a phase coupled simple scheme, a least squares cell based first order upwind spatial discretization, and a first order implicit transient formulation were employed. The spouted air and lettuce particulates were set as primary phase and secondary phase, respectively. The interactions between air and particulates were considered as drag and collisions of granular flow.

A structure mesh was generated by using a grid generation ANSYS ICEM. In the flow passage, the mesh contained 370,000 cells. The minimum size of cell was 0.01 mm. Comparisons of the coarser mesh model (70,000 cells), the mid-mesh model (370,000 cells) and the refined mesh model (750,000 cells) were carried out to ensure that the computational results were independent of mesh size. The failure of the coarser-mesh may be caused by bad transition elements.

<Figure.2>

Boundary conditions were defined as follows. The inlet was specified as velocity inlet, and the primary phase velocity is specified. The inlet spouting gas is specified as an ideal gas under the atmosphere pressure, whose properties were calculated by ideal gas state equation. The outlet was specified as vacuum pressure outlet. The gravity and volume fraction of particles were specified. The detailed numerical parameters of granular flow of lettuce particles are listed in Table 1. The instantaneous time step was set 0.001 s. Numerical simulations were carried out at the different spout gas velocities (u_{spout} =3.5 m/s, 7 m/s, 14 m/s, 28 m/s, and 56 m/s respectively).

< Table 1>

4. Results and discussion

To investigate the elevation characteristics of the spout fluidized lettuce particles, the hydrodynamics of the gas-solid spout fluidized bed with an increasing uniform inlet gas velocity were simulated.

4.1. Validation of the model

In order to validate this model to obtain the minimum fluidization in the spout fluidized bed, the minimum fluidization velocity was identified with the spout velocity of 3.5 m/s. The solid volume fraction, the phase 2 velocity and pressure at the minimum fluidization velocity were shown in Figure 3, Figure 4 and Figure 5. The lettuce particles kept the traditional fixed-bed state after running for 1s when the inlet gas velocity was equal to or smaller than the minimum fluidization velocity.

It was observed that the whole fluidization process in a spout fluidized bed included an initial stage and a steady stage (Figure 3, Figure 4 and Figure 5). The initial stage was an instantaneous developing process where the jet flow penetrated the bed, in which the jet appeared originally and then broke up periodically into bubbles without interference. The second stage was a steady circulation process where the particles circulated in a fixed pattern. A suspending surface of particles was formed at a height of 0.029 m from the inlet at spout velocity u_{spout} = 3.5 m/s. Most particles occupied the bottom and few particles were able to escape from this surface; the maximum particle velocity was up to 0.1 m/s.

<Figure.3>

<Figure.4>

<Figure.5>

4.2 Flow pattern

With the inlet spout gas velocity increase, the hydrodynamics of the gas-solid spout fluidized bed began to change. The flow pattern in a long vacuum cavity could be considered as a single jet, flow transition, and flow coalescence based on the frame-by-frame analysis (Guo et al. 2001 and Hong et al. 2003), which was simplified as a pseudo-2D cavity in this study. The detailed description of the flow pattern in wider operation conditions was presented below. The single jet characteristic was observed at a very low fluidized velocity, such as spout gas velocity 3.5 m/s as shown in Figure 3, Figure 4 and Figure 5.

4.2.1 Flow stability

Figure 6 shows the static pressure at the middle point located at the initial particle surface at different spout gas velocity. There was a clear unsteady initial process for about 1s, and after this fluctuating stage it tended to become steady when the gas spout velocity was lower than 21m/s. The duration of the unsteady status increased with the increase of spout velocity, and the pressure value tended to decrease and fluctuated as gas spout velocity increased. The particle velocity at the same point is shown in Figure 7. The particle velocity varied sharply at the initial stage, and became steady when spout velocity was lower than 21 m/s. When spout velocity was up to 28 m/s, particle velocity increased and was characterized by periodical fluctuation, and the fluidization presented an oscillatory nature. The above findings indicated that the spout velocity was an important factor in a spout fluidized bed. The whole process could be divided into two stages: a start-up stage and a quasi-steady fluidization stage.

<Figure.6>

<Figure.7>

4.2.2. Particle flow developing process

Considering the fluctuation characteristics of particle flow when spout velocity was up to 28 m/s, the particle flow patterns at spout velocity u_{spout} = 14 m/s and 28 m/s were discussed respectively to verify a key spout velocity affecting transition of the flow pattern, i.e. critical velocity. The effect of geometry structure of 2D spout fluidized bed on particle flow pattern was also evaluated.

Figures 8 and 9 show the instantaneous particle flow pattern during spout time of 3.0 s at spout velocity of u_{spout} = 14 m/s. The instantaneous particle flow patterns at the initial time of 1.0 s were obtained. It was noted that compared with spout velocity 3.5 m/s, the jet appeared and developed with more and stronger bubbles, causing more motion of the particles in the annulus region. Although most particles were elevated by spout gas flow, a small portion of particles was found near the wall of the air distributor. The occupancy of particles occurred near the bottom of the air distributor, and formed a spherical region. During the spout time from 1.0 s to 3.0 s with a 0.5 s interval, the distribution of particle velocity and maximum suspending height were shown in Figure 9. When the particle flow pattern was in a steady status, a suspending surface of particles was formed at a height of 0.045 m above the nozzle. Most high particle velocities were located at the upper region of air distributor with a spherical feature, which indicated that there were two particle circulation tracks in the spout fluidized bed. Few particles escape from the suspending surface and the maximum value of particle velocity was up to 0.26 m/s in the present study.

<Figure.8>

< Figure.9>

< Figure.10>

< Figure.11>

The instantaneous particle flow pattern at spout velocity u_{spout} = 28 m/s was obtained as shown in Figures 10 and 11. The instantaneous flow patterns at the initial time of 1.0s indicated that the jet rapidly appeared with more and stronger bubbles, penetrated the particle bed, and developed with significant elevation of most particles. The particles that accumulated on the wall of the air distributor were carried to the upper region as spout jet flow developed. Under this condition, the spout jet flow caused the motion of most particles in the annulus and axial regions. When spout velocity was up to 28 m/s, the particle flow pattern fluctuated and suspending height of particles was formed in a height range from 0.15 m to 0.25 m above the nozzle where the particle flow tended to be unsteady (Figure 11). Compared with particle flow at spout velocity of u_{spout} = 14 m/s, the maximum value of particle velocity was up to 1.63 m/s, and location of the higher velocity particles moved to the upper region at a height range from 0.02 m to 0.1 m. There was a narrow region with low particle velocity, which might have been caused by main spout gas flow.

The characteristics of flow patterns at different spout velocities indicated that there was a correlation between spout gas flow velocity and particle status. There was a critical velocity in which effect transition of the flow pattern occurred as the spout velocity increased.

4.3. Effect of spout velocity on particle circulation pattern

The particle circulation during drying indicates the particle mixing, and affects the heat and mass transfer between different particles in a spout fluidized bed in a microwave-assisted vacuum drying cavity. Penetration characteristics of spout gas flow and particle movement were investigated to understand the effect of spout velocity on particle circulation pattern in a pseudo-2-D spout fluidized bed.

4.3.1. Penetration of spout fluidization in a pseudo-2-D spout fluidized bed

In a spout fluidized bed, no matter whether the gas leaves the nozzle as bubbles, pulsating jet, or permanent jet, the fact is that there exists extensive gas and solid mixing in the jet region (Hong et al. 2003). The jet penetration depth is a key parameter to characterize the spout gas flow, which increases with increasing jet gas velocity in the spout fluidized bed. The discrepancies among various models for predicating the jet penetration depth were essentially due to the different definitions of jet boundary (Musmarra, 2000). In this study, jet penetration depth was defined as the contour line of voidage as 0.8 (Gidaspow and Ettehadleh 1983). Figure 12 shows the influence of spout gas velocity on the penetration depths and pressure drop in a 2D vacuum cavity. The penetration depth increased slowly below the spout gas velocity of 28 m/s, and then increased rapidly until 56 m/s. There was an approximately linear correlation between the jet penetration depth and gas spout velocity.

The bed pressure drop is another important parameter for characterizing the particle circulation pattern in a vacuum fluid bed dryer, defined as pressure difference (ΔP) between the inlet and outlet of solid-gas mixture in the quasi-steady stage. The bed pressure drop at different spout gas velocity is present in Figure 12. The results indicated that the pressure drop changed from negative pressure to positive pressure, when the spout gas velocity increased from 14 m/s to 21 m/s. This phenomenon suggested a significant change of particle circulation pattern that the elevated force acting on particles by the spout gas flow has overcome the gravity of particles, and particles begin to be elevated from the bottom of air distributor to the upper region of the vacuum cavity. Therefore, the velocity range from 14 m/s to 28 m/s was a critical velocity region to influence the particle circulation pattern.

<Figure.12>

4.3.2. Particles movement

Because the particle movement maintained similar features when the spout fluidized process enters the quasi-steady stage (spout time is generally over 1 s), the effect of spout velocity on the particle movement at spout time 3.0 s was analyzed. The distribution of particle volume fraction at t = 3.0 s is shown in Figure 13. The particle volume fraction was defined as the percentage of the volume the lettuce particles occupied in the drying cavity. When the spout velocity was 7 m/s, most particles accumulated near the air distributor, and only a small amount of particles moved up. As the spout velocity increased to 14 m/s, most particles participated in an upside movement, and formed a ball like distribution, though the particles were still around the air distributor. When the velocity was increased to 21 m/s and 28 m/s, the particles' movements expanded to a distance of about 0.2 m from the air distributor and most particles were located in this region. Finally, when the velocity was 56 m/s, some particles moved up to the height of 0.5 m, and most of them were located 0.2 m above the jet nozzle. The results indicated that, at a constant amount of particles, particle distribution was controlled by the spout gas velocity. This information might be helpful to improve the microwave-assisted spout fluidized bed heating to obtain a uniform particle temperature.

< Figure.13>

Figure 14 shows the particle flow patterns under different spout velocities at t = 3.0 s and the same amount of particles. The particle velocity increased from 0.1 m/s to 3 m/s with the increased spout velocity. Although the velocity distribution in the upper region above the particle suspending surface was observed at low spout velocity (u_{spout} = 7 m/s, 14 m/s), the particles' movements were mainly maintained below the particle suspending surface, and few particles were existed in the region above the particle suspending surface according to the distribution of the particle volume fraction. With the increase in spout velocity and development of a spout jet flow, particles accumulated on the wall of the air distributor were carried to the upper region. When spout velocity was increased to 56 m/s, the particle movement was more spacious and significantly different from that of the transitional fluidized bed. Below this spout velocity, most particles moved up instantaneously, and some of them moved out of the vacuum cavity, while no apparent particle suspending surface was observed. Although there was a higher particle velocity in the region with a height range from bottom to 0.2 m, the effect of these particles was slight because there were few particles in this region according to the distribution of particle volume fraction.

< Figure.14>

The results showed that the particle circulation pattern was different under different gas spout velocities. In a spout fluidized bed in a microwave-assisted vacuum dryer, the particle circulation pattern was one of the important factors affecting the heating uniformity. A spacious particle distribution was beneficial to obtain uniform microwave energy, and improve convective heat transfer under fluidization.

5 Conclusions

In the present study, the TFM method was verified to successfully obtain the gas-particle flow in this pseudo-2-D spout fluidized bed in a vacuum drying cavity. The dynamic characteristics of spout fluidized bed and the effect of spout elevation on particle movement at different operating conditions were obtained based on simulation results.

The model simulation illustrated that the spout fluidized process included isolated, merged and transitional jets when the spout gas velocity was increased. The isolated jet turned into the merged jet via the transitional jet. The fluidization at a certain velocity could be divided into two stages: a start-up stage and a quasi-steady fluidization stage. The spout velocity was an important factor controlling particle status in the spout fluidized bed. There was a critical velocity range from 14 m/s to 28 m/s where the particle flow pattern was changed from steady flow to unsteady flow.

There was an approximately linear correlation between the jet penetration depth and gas spout velocity. The pressure drop tended to convert from negative pressure to positive pressure as spout velocity increased up to the critical velocity. In the quasi-steady stage, particle circulation pattern significantly changed with increased spout velocity, and particles began to be elevated from the bottom of air distributor to the upper region of the vacuum drying cavity.

Acknowledgements

The authors thank the China 863 HI-TECH Research and Development Program (No. 2011AA100802), China Postdoctoral Program, and Natural Science Foundation of Jiangsu Province (Grant No: BK20130150) for financial supports. The authors also thank Mr Paul Dubois, from Curtin University, for his professional English editing.

References

Bouillard J., Lyczkowski R., &Gidaspow D. (1989). Porosity distributions in a fluidized bed with an immersed obstacle, *AIChE Journal*, 35, 908-922.

Balakrishnan, M., Raghavan, G.S.V., Sreenarayanan, V.V., &Viswanathan, R. (2011). Batch drying kinetics of cardamom in a two-dimensional spouted bed. *Drying Technology*, 29(11), 1283-1290.

de Jesus, S.S. & Filho, R.M. (2011). Optimizing drying conditions for the microwave vacuum drying of enzymes. *Drying Technology*, 29(15), 1828-1835.

Feng, H. & Tang, J.(1998). Microwave finish drying of diced apples in a spouted bed. *Journal of Food Science*, 63(4), 679-683.

Feng H., Tang J., Cavalieri R. P., &Plumb O. A.(2001). Heat and mass transport in microwave drying of porous materials in a spouted bed, *AIChE Journal*, 47(7), 1499-1512.

Garside, J. & Al-Dibouni, M. R.. (1977). Velocity-voidage relationships for fluidization and sedimentation. Industrial & Engineering Chemistry Process Design and Development, 16, 206-214.

Giri, S.K. & Prasad, S. (2007). Drying kinetics and rehydration characteristics of microwave vacuum and convective hot-air dried mushrooms. *Journal of Food Engineering*, 78, 512-521.

Gidaspow, D. & Ettehadleh, B. (1983). Fluidization in two-dimensional beds with a jet. 2. Hydrodynamic modeling. *Industrial & Engineering Chemistry Fundamentals*, 22(2), 193-201.

Gidaspow, D. (1994). Multiphase flow and fluidization: Continuum and kinetic theory description. New York: Academic Press.

Gidaspow, D., Jung, J., &Singh, R. (2004). Hydrodynamics of fluidization using kinetic theory: an emerging paradigm: 2002 Flour-Daniel lecture. *Powder Technology*, 148, 123-141

Guo, Q., Tang, Z., Yue, G., Liu, Z., & Zhang, J. (2001). Flow pattern transition in a large jetting fluidized bed with double nozzles. *AIChE Journal*, 47(6), 1309–1317.

Hu, Q., Zhang, M., Mujumdar, A.S., Xiao, G., Sun, J. (2006). Drying of edamames by hot air and vacuum microwave combination. *Journal of Food Engineering*, 77(4), 977-982.

Huang, L. L., Zhang, M., Mujumdar, A.S., & Sun, X.L. (2011). Comparison of four drying methods for re-structured mixed potato with apple chips. *Journal of Food Engineering*, 103, 279-284.

Han, Q. H., Yin, L. J., Li, S. J., Yang, B. N., &Ma, J. W. (2010). Optimization of process parameters for microwave vacuum drying of apple slices using response surface method. *Drying Technology*, 28(4), 523-532.

Hong, R., Guo, Q., Luo, G., Zhang, J., & Ding, J. (2003). On the jet penetration height in fluidized beds with two vertical jets. *Powder Technology*, 133(1), 216-227.

Jangam, S.V. (2011). An overview of recent developments and some R&D challenges related to drying of foods. *Drying Technology*, 29(12), 1343-1357.

Jambhale A.S. & Barbadekar B.V. (2008). Microwave drying system with high-tech phase controller: a modified applicator. *World Academy of Science, Engineering and Technology*, 46, 1-5.

Li, Z. Y., Wang, R. F., & Kudra, T. (2011). Uniformity issue in microwave drying. *Drying Technology*, 29(6), 652-660.

Musmarra, D. (2000). Influence of particle size and density on the jet penetration length in gas fluidized beds. *Industrial & Engineering Chemistry Research*, 39(7), 2612-2617.

Nahimana, H. & Zhang, M. (2011). Shrinkage and color change during microwave vacuum drying of carrot. *Drying Technology*, 29(7), 836-847.

Rahimi, M. R., Azizi, N., Hosseini, S. H., & Ahmadi, G. (2013). CFD study of hydrodynamics behavior of a vibrating fluidized bedusing kinetic-frictional stress model of granular flow, *Korean Journal of Chemical Engineering*, 30(3), 761-770.

Pai M., Subramaniam S. (2009). A comprehensive probability density function formalism for multiphase flows. *Journal of Fluid Mechanics*, 628, 181-228.

Pritchett J., Blake T., &Garg S.(1978). A numerical model of gas fluidized beds, in: *AIChE symposium series*, volume 176, 134-148.

Pei, P., Zhang, K., Lu, E., & Wen, D. (2009). CFD simulation of bubbling and collapsing characteristics in a gas–solid fluidized bed. *Petroleum Science*, 6(1), 69–75.

Passalacqua, A. & Marmo, L. (2009). A critical comparison of frictional stress models applied to the simulation of bubbling fluidized beds, *Chemical Engineering Science*, 64(12), 2795-2806.

Syamlal, M. & O'Brien, T. J. (1989). Computer simulation of bubbles in a fluidized bed. *AIChE symposium series*, 85:22-31.

Shen, C.(2005). Rarefied gas dynamics: fundamentals, simulations and micro flows, Publisher: Springer-Verlag Berlin and Heidelberg GmbH & Co. K.

Torringa H.M., Dijk E. J. V., & Bartels P.V. (1996). Microwave puffing of vegetables: modeling and measurements. *In: Proceedings of 31st microwave power symposium*, 16-19.

Vennerstrum, S. (1989). Microwave Vacuum Dryer. U.S. Patent No. 4,856,203.

Vadivambal, R.& Jayas, D.S.(2010). Non-uniform temperature distribution during microwave heating of food materials-A review. *Food and Bioprocess Technology*, 3, 161-171

Wang, Y., Zhang, M., Mujumdar, A.S., Mothibe, K. J., & Roknul Azam, S. M. (2013). Study of Drying Uniformity in Pulse-Spouted Microwave-Vacuum Drying of Stem Lettuce Slices with Regard to Product Quality. *Drying Technology*, 31(1), 91-101.

Wang, Y., Zhang, M., Mujumdar, A.S., & Mothibe, K. J. (2013) Microwave-assisted pulse-spouted bed freeze-drying of stem lettuce slices-effect on product quality, *Food and Bioprocess Technology*, 6:3530-3543

Wang, Y., Zhang, M., Mujumdar, A.S., & Mothibe, K.J. (2012). Experimental investigation and mechanism analysis on microwave freeze drying of stem lettuce cubes in a circular conduit. *Drying Technology*, 30 (11-12), 1377-1386.

Wang, Q., Zhang, K., Sun, G., Brandani, S., Gao, J., & Jiang, J. (2007). CFD simulation of fluid dynamics in a gas–solid jetting fluidized bed. *International Journal of Chemical Reactor Engineering*, 5, A112.

Zhang, M., Tang, J., Mujumdar, A.S., & Wang, S. (2006). Trends in microwave-related drying of fruits and vegetables. *Trends in Food Science & Technology*, 17(10), 524-534.

Zhang, M., Jiang, H., & Lim, R.-X. (2010). Recent developments in microwave-assisted drying of vegetables, fruits, and aquatic products-drying kinetics and quality considerations. *Drying Technology*, 28(11), 1307-1316.

Zhong, W., Zhang, Y., & Jin B. (2010). Novel method to study the particle circulation in a flatbottom spout-fluid bed. *Energy and Fuels*, 24, 5131–5138.

Table 1

Physical and numerical parameters of the particle and gas used in the experiment

Particle phase		**Gas phase**	
Particle	Lettuce	Fluid	Air
Diameter, d_p (mm)	0.005	Inlet gas density, ρ_g (kg/m^3)	1.205
Density, ρ_g (kg/m^3)	1387	Viscosity, μ_g (Pa/s)	18.1×10^{-6}
Volume fraction	0.003	Cavity height, H (mm)	516
Granular viscosity(Pa/s)	Syamlal-Obrien drag model	Vacuum pressure(Pa)	7000
Granular bulk viscosity(Pa/s)	Lun-et-al model	Air distributor angle, (º)	45
Frictional Viscosity(Pa/s)	Schaeffer,Johnson-et-al model	Nozzle width, L(mm)	8
Granular Temperature(m^2/s^2)	algebraic model	Grid number	370,000
Solid pressure(Pa)	Lun-et-al model	Grid type	Structure
Radial Distribution	Lun-et-al model	Time step, Δt (s)	1×10^{-3}
Elasticity Modulus(Pa)	Lun-et-al model		
Packing limit	0.63		

Figure captions

Figure.1 Schematic diagram of a pulsed spouted microwave-vacuum drying system

Figure.2 Computational models of air distribution structure

Figure.3 Particle volume fraction at the minimum spout fluidization velocity (u_{spout}= 3.5m/s, t = 0.2s-1.0s)

Figure.4 Pressure at the minimum spout fluidization velocity (u_{spout} =3.5m/s, t=0.2s-1.0s)

Figure.5 Particle velocity (u_{spout} = 3.5m/s, t =1.0s-3.0s)

Figure.6 Fluctuation of static pressure at different spout gas velocity

Figure.7 Fluctuation of particle velocity at different spout gas velocity

Figure.8 Particle volume fraction at the critical spout fluidization velocity at initial stage (u_{spout} = 14m/s, t = 0.1s-1.0s)

Figure.9 Particle velocity distribution at different spout time (u_{spout} = 14m/s)

Figure.10 Particle volume fraction distribution during spout time from 0.1s-1.0s (u_{spout} = 28m/s, t = 0.1s-1.0s)

Figure.11 Particle velocity (u_{spout} = 28m/s) of separation surface position

Figure.12 Penetration depth and pressure drop for a 2D vacuum cavity

Figure.13 Contour plot of the particle volume fraction in pseudo-2D spout fluidized bed at different spout velocity at t = 3.0s

Figure.14 Contour plot of the particle velocity in pseudo-2D spout fluidized bed at different spout velocity at steady stage (t = 3.0s)

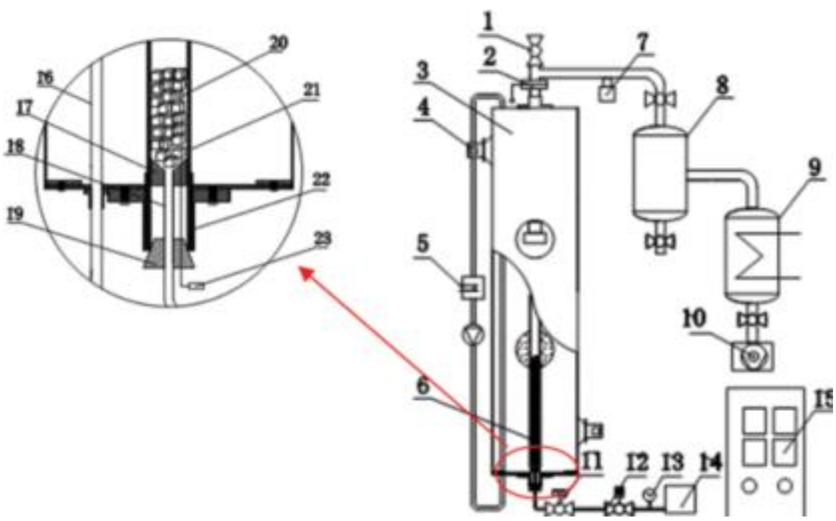

Figure.1 Schematic diagram of a laboratory pulsed spouted microwave-vacuum drying system

1 feeding ball valve, 2 plate valve, 3 microwave heating cavity, 4 magnetron, 5 circulating water unit, 6 drying chamber, 7 and 13pressure gauge, 8 solid–gas separator, 9 vapor condenser, 10 vacuum pump unit, 11 gas flow electromagnetic valve, 12 gas flow adjustable valve, 14 gas source, 15 control panel, 16 water load pipe, 17 gas distributer, 18 spout pipe, 19 silicon rubber stopper, 20 sample, 21 drying chamber, 22 fixed unit, 23 fiber optic temperature sensor

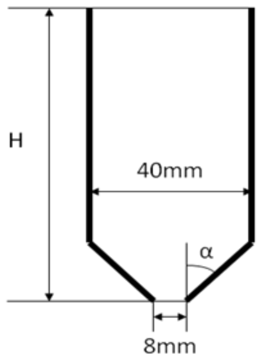

Figure.2 Computational models of air distribution structure

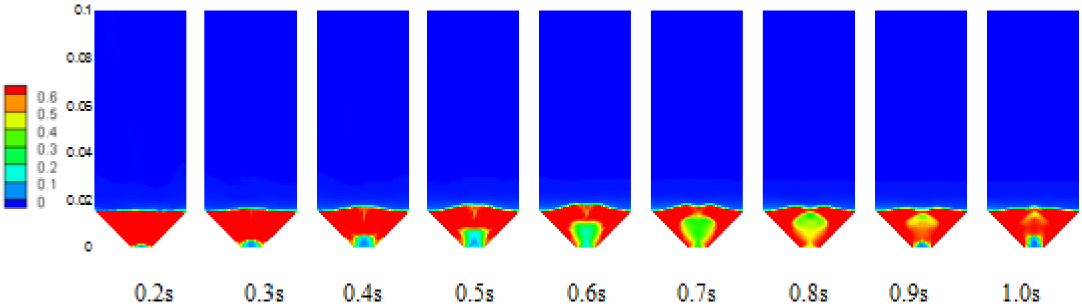

Figure.3 Particle volume fraction at the minimum spout fluidization velocity

(u_{spout} = 3.5m/s, t = 0.2s-1.0s)

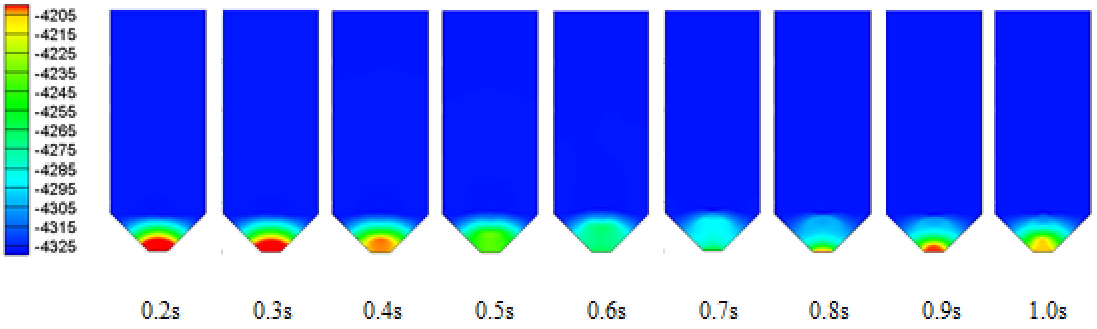

Figure.4 Pressure at the minimum spout fluidization velocity

(uspout =3.5m/s, t=0.2s-1.0s)

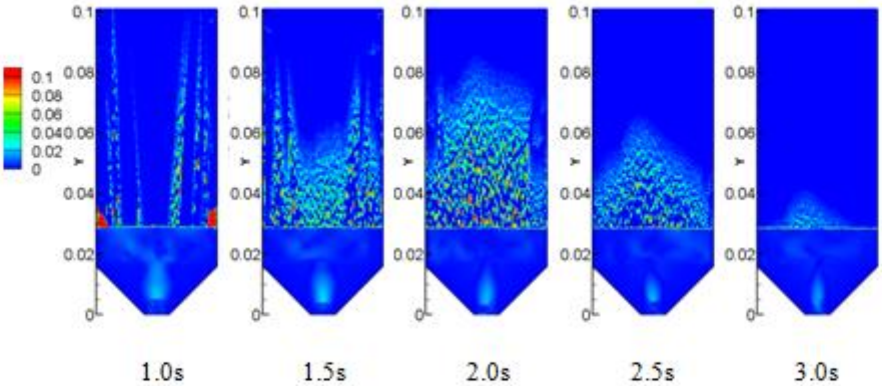

Figure.5 Particle velocity (u_{spout} =3.5m/s, t=1.0s-3.0s)

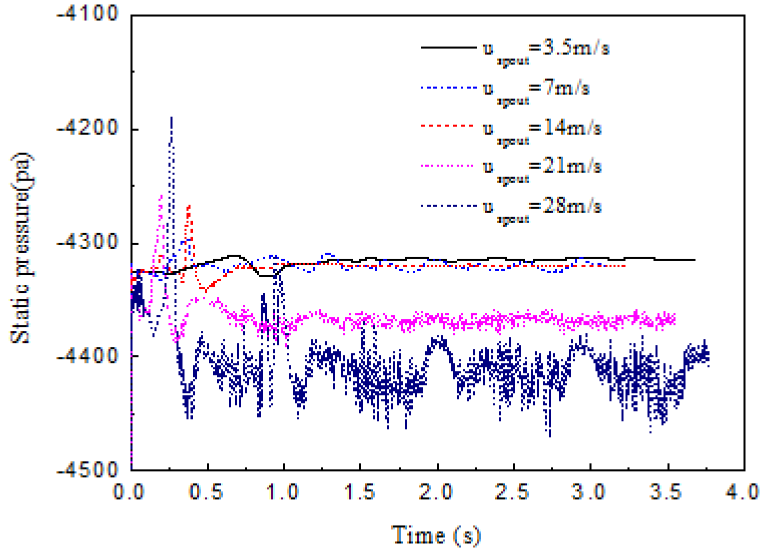

Figure. 6 Fluctuation of static pressure at different spout gas velocity

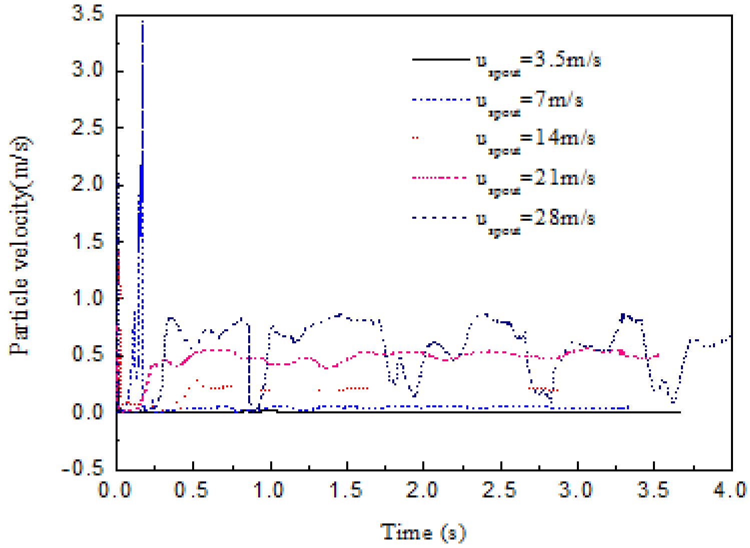

Figure. 7 Fluctuation of particle velocity at different spout gas velocity

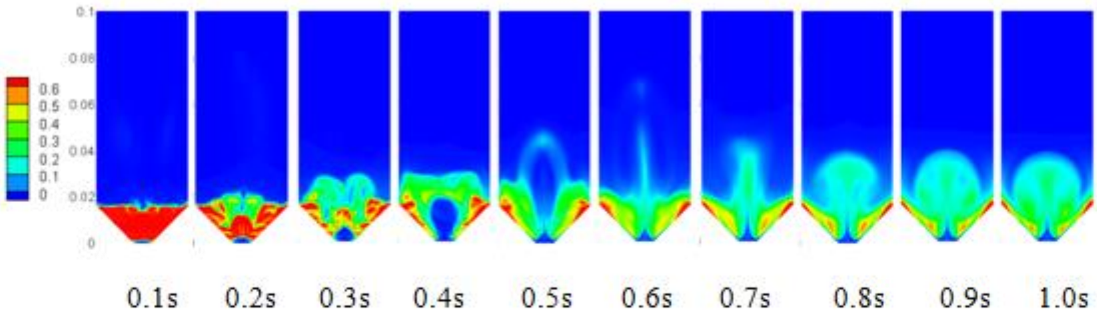

Figure.8 Particle volume fraction at the critical spout fluidization velocity at initial stage

(u_{spout} = 14m/s, t = 0.1s-1.0s)

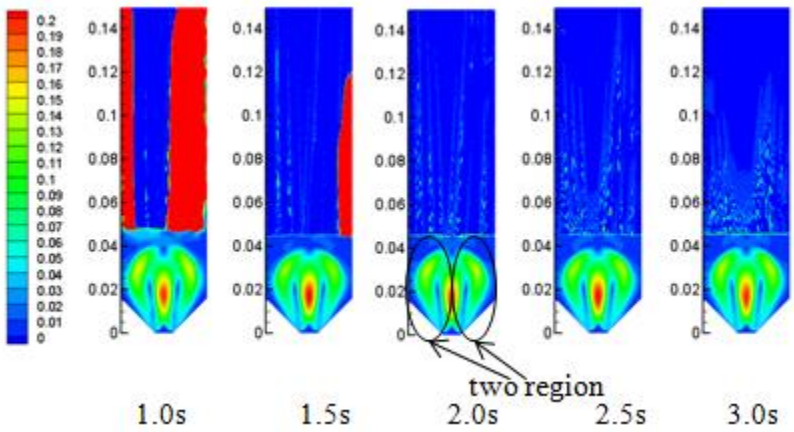

Figure.9 Particle velocity distribution at different spout time (u_{spout} =14m/s)

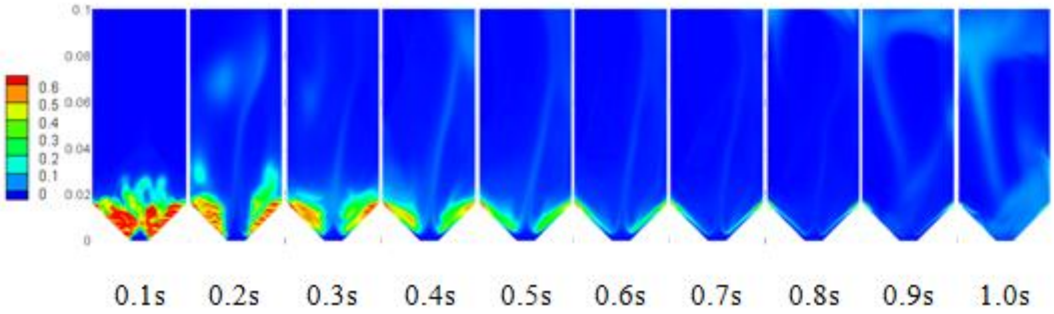

Figure.10 Particle volume fraction distribution during spout time from 0.1s-1.0s

(u_{spout} = 28m/s, t = 0.1s-1.0s)

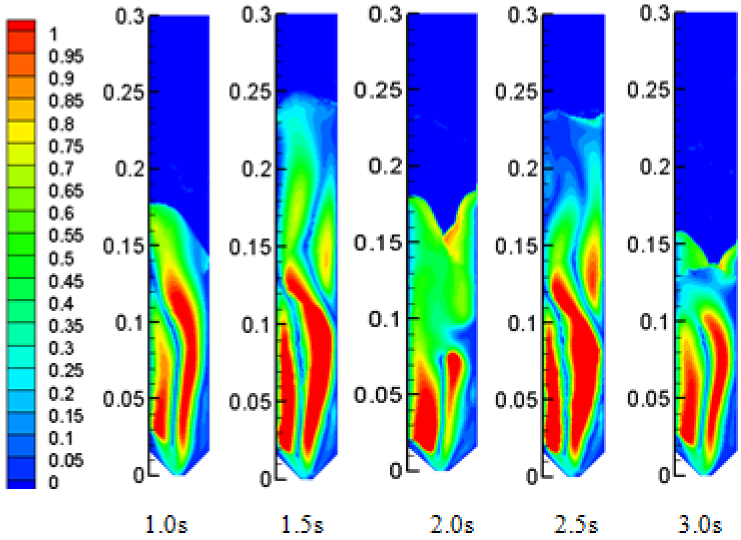

Figure.11 Particle velocity (u_{spout} =28m/s) of separation surface position

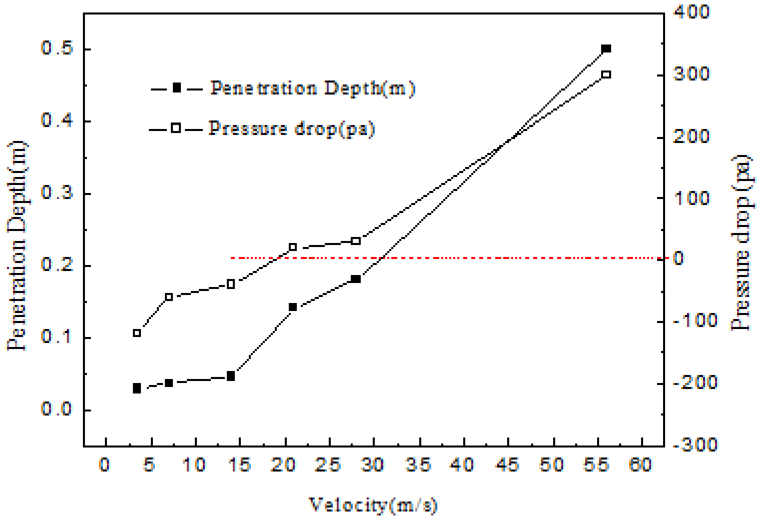

Figure. 12 Penetration depth and Pressure drop for a 2D vacuum cavity

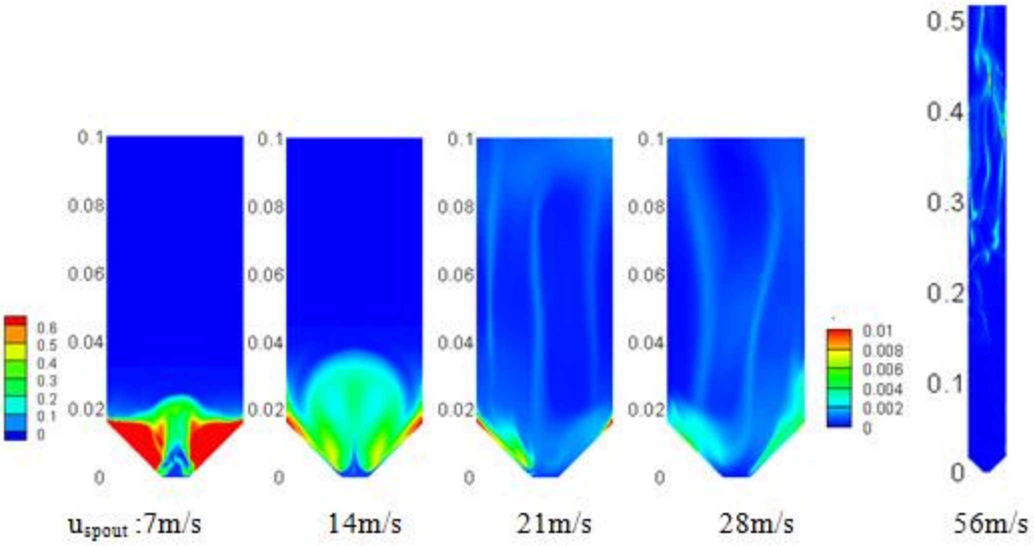

Figure.13 Contour plot of the particle volume fraction in pseudo-2D spout fluidized bed at different spout velocity at t=3.0s

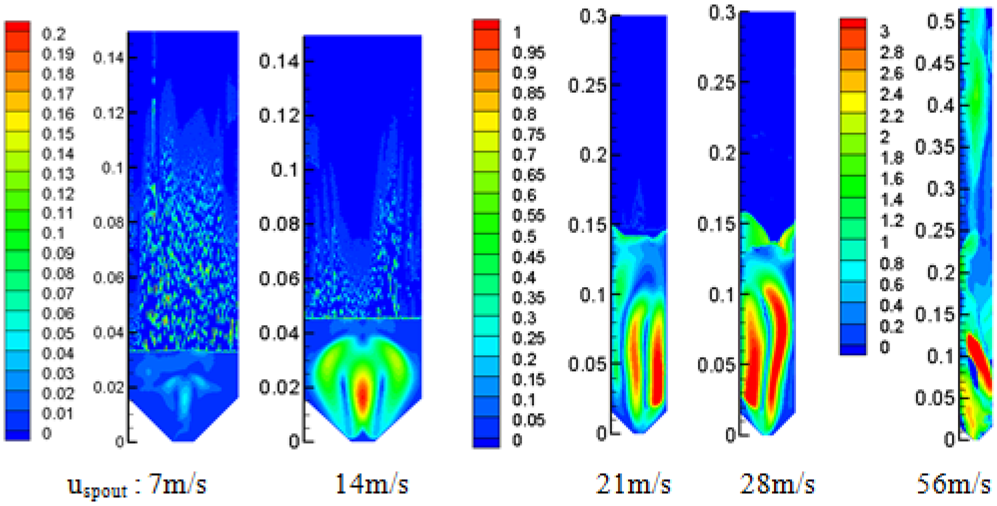

Figure. 14 Contour plot of the particle velocity in pseudo-2D spout fluidized bed at different spout velocity at steady stage (t=3.0s)